Journal of Alloys and Compounds 893 (2021) 162135

Contents lists available at ScienceDirect

Journal of Alloys and Compounds

journal homepage: www.elsevier.com/locate/jalcom

Modeling of the hydrogen sorption kinetics in an AB_2 laves type metal hydride alloy

Arif Hariyadi[a,b], Suwarno Suwarno[b,*], Roman V. Denys[c], Jose Bellosta von Colbe[d], Tor Oskar Sætre[a], Volodymyr Yartys[c,*]

[a] University of Agder, Faculty of Engineering and Science, Grimstad, Norway
[b] Department of Mechanical Engineering, Institut Teknologi Sepuluh Nopember (ITS), Kampus ITS Sukolilo, Surabaya, Indonesia 60111
[c] Institute for Energy Technology (IFE), Kjeller, Norway
[d] Helmholtz-Zentrum Hereon, Geesthacht, Germany

ARTICLE INFO

Article history:
Received 3 August 2021
Received in revised form 22 September 2021
Accepted 25 September 2021
Available online 28 September 2021

Keywords:
Laves phase intermetallic
Metal hydride
Kinetics
Phase-structural transformation
Solid-state reaction

ABSTRACT

Hydrides of the AB_2 Laves type alloys (A=Zr, Ti; B = transition metal – Fe, Co, Ni, Mn, Cr, V) have been extensively studied as materials for the storage of gaseous hydrogen. They contain up to 4 H atoms/formula unit AB_2, thus achieving reversible H storage capacities in the range between 1.5 and 2.0 wt% H and offering high rates of hydrogen charge and discharge, thus making them suitable for designing efficient hydrogen stores operating at ambient conditions. In the present study, we performed an experimental study and modeling of the thermodynamics and the kinetics of interaction in the AB_2-hydrogen system. The experimental data was collected by studying a model alloy with a composition $Ti_{0.15}Zr_{0.85}La_{0.03}Ni_{1.126}Mn_{0.657}V_{0.113}Fe_{0.113}$. Hydrogen absorption and desorption were studied in a volumetric Sieverts type apparatus at isothermal conditions using a single-step change/discharge and stepwise methods. The results obtained from the model simulation show that the reaction follows the Johnson-Mehl-Avrami-Kolmogorov (JMAK) model, with the value of exponent n = 1–1.25 for absorption and 1 for desorption. This indicates that the rate-limiting hydrogen absorption and desorption steps are jointly governed by hydrogen diffusion and grain boundary nucleation of alpha-solid solution and beta-hydride. The activation energies for both hydrogen absorption and desorption decrease along with increasing hydrogen content in the hydride.

1. Introduction

The need for energy storage is increasing because of the extensive development of renewable energy technologies. As an example, in the power sector, the share of renewable energy will rise from 25% in 2015 to 85% in 2050, with the highest growth estimated for wind and solar energy when using photovoltaic (PV) panels [1]. However, wind and solar power generation produce intermittent electrical energy, and this production fluctuation has to be stabilized either with the energy from another type of renewables or by using primary energy (hydropower or fossil fuel) utilization or by the energy accumulated in the energy storage system. Importantly, the requirements for energy storage in an off-grid power system should meet the power demand of the system.

Batteries are considered ideal energy storage devices, but in the case of long-term or seasonal energy storage, batteries have limitations caused by the energy loss due to a self-discharge, further to a high cost of the battery system together with a limited energy storage capacity. These limitations can be overcome by using hydrogen. Hydrogen is considered as an energy carrier obtained utilizing excess seasonal photovoltaic or wind power. In the electrolyzer, electricity is converted to hydrogen, and during the winter or low wind season, the hydrogen stored can be converted back to electricity in a fuel cell [2]. The use of metal hydride systems for hydrogen storage in portable, stationary, and mobile applications [3,4], and when combined with fuel cell has been reviewed in [5]. A challenge for the various metal hydride-based hydrogen storage applications integrated with fuel cells is in developing H storage systems with good kinetics. In other words, a hydrogen storage tank is expected to provide a specific flow rate of hydrogen supply sufficient for a normal operation of a fuel cell [6].

* Corresponding authors.
E-mail addresses: warno@me.its.ac.id (S. Suwarno), volodymyr.yartys@ife.no (V. Yartys).

https://doi.org/10.1016/j.jallcom.2021.162135
0925-8388/

Studies of hydrogen absorption and desorption kinetics are essential for the optimization of the practical hydrogen storage system performances, reaching advances in materials development, and for the improvement of the fundamental understanding of hydrogen uptake and release mechanisms. Kinetics of the alloy's interaction with H_2 can be studied by using the H_2 pressure and temperature-dependent modeling approach, thus allowing to successfully describe the Metal - H_2 interactions. In many cases, the kinetics study assists in identifying the reaction mechanisms and the limiting steps of hydrogen absorption and desorption. For the mechanism of the reactions, the selection of certain applied models depends on the type of the studied materials and their characterization conditions. The common features of various models describing the kinetics of hydrogen absorption and desorption have been reviewed in [7]. If the limiting steps of the kinetic processes are identified, this assists in further optimizing materials development. As an example, the effect of catalysts [8,9] or microstructural optimization can be determined [10,11].

For the hydrogen absorption kinetics, many models have been earlier studied and reviewed [7]. One of the well-known models is a nucleation and growth Johnson-Mehl-Avrami-Kolmogorov (JMAK) model. This model has been known for decades and is able to describe and to predict the kinetics of solid-state transformations in the alloys, including hydrogen absorption kinetics. However, many studies using this model were performed at the conditions when the thermodynamic influence can be neglected. When the pressure is largely varied, the impact of the overall kinetics during the hydrogen absorption and desorption study becomes essential.

The AB_2 alloys belong to a large and well-studied hydrogen storage materials Laves type group of the alloys. As A metals, they contain Ti, Zr, Ta, Hf, while the B elements include transition metals such as Fe, Co, Ni, Mn, Cr, V, and have been known since the '80s [12]. The Zr-based AB_2 alloys show sluggish hydrogen absorption kinetics, while the rare earth metals (including mischmetal) when added to AB_2 alloys, improve activation behaviors of the alloys [13,14]. The addition of small amounts of La to the composition of AB_2 alloys has also been studied and has been found to improve the electrochemical performance of the alloys [15–17]. The effect was caused by the presence of a secondary phase of a LaNi type catalyzing the kinetics of the electrochemical hydrogen absorption. While the electrochemical studies have already been reported, a detailed research on the gas phase hydrogenation kinetics has not been done.

In the present work, we focus on studies of one type of these alloys, $Ti_{0.15}Zr_{0.85}La_{0.03}Ni_{1.126}Mn_{0.657}V_{0.113}Fe_{0.113}$, containing additions of La for the improvement of the activation performance and cycling stability. The model alloy was selected based on our in-house research of $AB_{2\pm x}$ C15 Laves-type alloys for their application as hydrogen storage and battery electrode materials. In multi-element $AB_{2\pm x}$ alloys, constituting elements contribute to the H storage performance in a variable way. Indeed, Ti, Zr, and V are the hydrides forming elements, Ni has a high catalytic activity, Co and Mn provide surface activity relevant for the improvement of hydrogen exchange, and Cr, Al, and Fe increase alloys stability in hydrogen. We performed an experimental and modeling study on hydride sorption kinetics using the general approach while further developing it by introducing pressure- and temperature-dependent rates of transformations. We assessed various reaction kinetics models for the solid-state reactions and selected the most suitable one. This study describes the formation and decomposition of metal hydrides and is useful for optimizing metal hydride tanks using AB_2 materials and their operation during hydrogen charge and discharge.

2. Methods

The studied AB_2 alloy was synthesized using an Edmund Buehler arc melter. The alloy with a composition $Ti_{0.15}Zr_{0.85}La_{0.03}Ni_{1.126}Mn_{0.657}V_{0.113}Fe_{0.113}$ was prepared from the commercially available individual elements. The purity of each constituent element was higher than 99.7%. The arc melting was performed on a water-cooled copper hearth under an inert gas atmosphere (argon), while the alloy was remelted three times to improve its homogeneity. The alloy was annealed at 950 °C for 24 h before its quenching into a mixture of ice and water. This alloy has also been studied earlier [18], and it showed to be a phase-pure material crystallizing with a C15 FCC Laves type structure and a unit cell parameter a = 7.0338(6) Å.

Hydrogenation-dehydrogenation studies were performed using a Sievert's type volumetric method. The sample was placed into a closed reactor of a known volume made from stainless steel. Hydrogen gas was supplied into the gas collector system of a known volume equipped with pressure transducers. The pressure was monitored to determine the molar content of hydrogen gas. When the valve between the collector and the reactor is opened, the amount of hydrogen gas absorbed can be determined from the change of the measured pressure in the system [19,20].

The PCT (Pressure-Composition-Temperature) and kinetics measurements were performed by using the sample with a mass of appr. 2 g and 100 mg, correspondingly. The alloy powder consisted of particles with a nonregular shape and an average size of 50 µm. The powdered sample was heated under vacuum at 573 K for 1 h and cycled several times for hydrogen absorption-desorption to reach the reproducibility of hydrogen storage capacity during H_2 absorption/desorption and to achieve high hydrogen exchange rates. Hydrogen gas with a purity of 99.999% was used during the experiments.

Two types of hydrogen sorption experiments were performed; the first one was a stepwise absorption/desorption at a plateau section of the phase diagram. Secondly, the measurement was conducted in a single step absorption/desorption experiment in which before absorption, a hydrogen-free powder was used, and otherwise, for the desorption, a fully hydrogenated sample was used [20]. Nickel foam (200 mg) was used as a heat sink to enhance the rates of heat exchange and to minimize the change in the sample temperature during the measurements. The measurements were performed at hydrogen pressures from 0.005 to 18.860 bar H_2 absolute, at four different constant temperature setpoints of 273 K, 293 K, 323 K, and 353 K.

Time-domain simulations, variable iterations, data fitting, and data processing were performed using numerical computing and proprietary, self-programmed code accommodated in Matlab®. The modeling stage started with a study of thermodynamics, kinetics, and reaction mechanism of the transformations in the metal-hydrogen system. Several selected mathematical models suitable to describe the transformations in the chosen metal hydride system were considered. Besides that, the effect of pressure and temperature was investigated using the data with the reaction starting at equal initial concentrations to assess the effects of temperature and pressure on the studied process. The PCT measurement data was used to build the PCT model to get the equilibrium pressure at any point of H_2 content. Equilibrium pressure at any concentration and temperature was needed to calculate the K(P) along with the driving force of the reaction.

The kinetics of the interaction defined by the dynamic behavior of the metal hydride during the phase transformation was considered by Førde et al. [20]. They showed that a good approximation of the reaction kinetics could be achieved using the integrated JMAK expression presented in Eq. (1):

$$X = 1 - \exp\left(-Kt^n\right) \quad (1)$$

where X is a reacted fraction, K is the rate constant, t is time, and n is a value ranging from 0.5 to 4, depending on the mechanism and growth dimensionality which were described in detail in [20].

The reacted fraction X is determined from the ratio of actual concentration C (hydrogen content), minimum concentration C_1, and a final maximum concentration C_2.

The reacted fractions for absorption and desorption are defined in Eqs. (1) and (2):

$$X = \frac{C - C_1}{C_2 - C_1} \text{ absorption} \tag{2}$$

$$X = \frac{C_2 - C}{C_2 - C_1} \text{ desorption} \tag{3}$$

This model splits the overall rate constant K into a pressure-dependent term K(P) and a temperature-dependent term K(T), as shown in Eq. (4):

$$K = K(P) \cdot K(T) \tag{4}$$

The temperature-dependent term K(T) is the Arrhenius equation, which is the function of energy activation E_a, a universal gas constant R, and rate constant for the temperature-dependent term K_0, which is expressed in Eq. (5):

$$K(T) = K_0 \exp\left(-\frac{E_a}{RT}\right) \tag{5}$$

Several pressure-dependent terms are present in the Eqs. (6)–(20) are used along with the reaction models as a factor to take into account the effect of pressure. The pressure-dependent term K (P) has been suggested from the analysis of the reference data for the metal hydride when formed/decomposed during a solid-gas reaction, depending on the rate-limiting step of the reaction:

a. Diffusion is the rate-limiting step (L1), K(P) is related to the square root of pressure [21]:

$$K(P) = 1 - \left(\frac{P_{eq}}{P}\right)^{0.5} \text{ absorption} \tag{6}$$

$$K(P) = 1 - \left(\frac{P}{P_{eq}}\right)^{0.5} \text{ desorption} \tag{7}$$

b. Chemisorption is the rate-limiting step (L2), K(P) is related to the difference between the gas pressure and the equilibrium pressure [22,23]:

$$K(P) = (P - P_{eq}) \text{ absorption} \tag{8}$$

$$K(P) = (P_{eq} - \mathrm{P}) \text{ desorption} \tag{9}$$

c. The rate of phase transformation is a rate-limiting step (L3), where K(P) is related to the natural logarithm of the quotient of operating and equilibrium pressure [24,25]:

$$K(P) = \ln\frac{P}{P_{eq}} \text{ absorption} \tag{10}$$

$$K(P) = \ln\frac{P_{eq}}{P} \text{ desorption} \tag{11}$$

d. The semi-empirical pressure normalization method (L4) [26,27] can be defined as:

$$K(P) = \left(\frac{P - P_{eq}}{P_{eq}}\right) \text{absorption} \tag{12}$$

$$K(P) = \left(\frac{P_{eq} - P}{P_{eq}}\right) \text{desorption} \tag{13}$$

e. Nucleation and growth of the alfa and beta phase are the rate-limiting step, K(P) is defined considering the reversible nature of the absorption/desorption reaction (L5), where alpha is constant [28]:

$$K(P) = \left(\frac{P}{P_{eq}}\right)^{\alpha} \text{absorption/desorption} \tag{14}$$

f. Bernauer et al. [29] investigated the diffusion of H-atoms as the rate-limiting step (L6):

$$K(P) = P^{0.5} \text{absorption/desorption} \tag{15}$$

g. Hydrogen diffusion through the hydride phase can be a rate-limiting step (L7) [25]:

$$K(P) = (P^{0.5} - {P_{eq}}^{0.5}) \text{absorption} \tag{16}$$

$$K(P) = ({P_{eq}}^{0.5} - P^{0.5}) \text{desorption} \tag{17}$$

h. K(P) is derived considering the contribution from the reverse reaction (e.g., product pressure) to the overall response (L8) [30]:

$$K(P) = \left(1 - \frac{P_{eq}}{P}\right) \text{absorption} \tag{18}$$

$$K(P) = \left(1 - \frac{P}{P_{eq}}\right) \text{desorption} \tag{19}$$

i. Koga et al. proposed a generalized form to describe the kinetic behavior at different pressure conditions, where a and b are constants (L9) [31]:

$$K(P) = \left(\frac{1}{P}\right)^{a}\left(1 - \left(\frac{P}{P_{eq}}\right)^{b}\right) \text{absorption/desorption} \tag{20}$$

Furthermore, it should be noted that the recommendations for performing kinetic computations on thermal analysis data by the Kinetics Committee of the International Confederation for Thermal Analysis and Calorimetry (ICTAC) [32] define the reaction rate as related to the temperature (T), the reacted fraction (X), and the pressure (P) as follows:

$$\frac{dX}{dt} = k(T) \quad f(X) \quad h(P) \tag{21}$$

Since the f(X) is the differential form of the reaction model equation [33]:

$$f(X) = \frac{1}{k}\frac{dX}{dt} \tag{22}$$

by rearranging the Eq. (21) we obtain:

$$\frac{dX}{dt} = k(T) \quad \frac{1}{k}\frac{dX}{dt} \quad h(P) \tag{23}$$

$$k = k(T) \quad h(P) \tag{24}$$

It can be concluded that the Eqs. (21) and (24) are the differential form of the Eq. (4) taking into consideration $f(X) = \frac{1}{k}\frac{dX}{dt}$.

Table 1
Rate laws for the reactions relevant for the description of the solid-state reactions during the formation-decomposition of the metal hydrides.

Label	Integral form g (X)=Kt	Definition
JMAK	$[-\ln(1-X)]^{\frac{1}{n}}$	Johnson-Mehl-Avrami-Kolmogorov (JMAK) nuclei growth
R1	$1-(1-X)^{2/3}$	One dimensional contraction
R2	$1-(1-X)^{1/2}$	Contracting area
R3	$1-(1-X)^{1/3}$	Contracting volume
D1	X^2	One-dimensional diffusion-controlled
D2	$(1-X)\ln(1-X)+X$	Two-dimensional diffusion-controlled
D3	$[1-(1-X)^{1/3}]^2$	Three-dimensional diffusion-controlled
D4	$[1-(2X/3)]-(X)^{2/3}$	Three-dimensional contracting volume with decelerated interface
F1	$-\ln(1-X)$	First order transformation
F2	$1/(1-X)$	Second order transformation
F3	$[1/(1-X)]^2$	Third-order transformation

Furthermore, several reaction models of solid-state reaction are relevant for the description of the kinetics of the processes of the formation-decomposition of metal hydrides [7,32] listed in Table 1.

When it comes to the model selection, we defined it using a linear dependence g(X)=Kt and used the K=K(P)·K(T) from the Eq. (4).

$$g(X)/K(P) = K(T)\cdot t \tag{25}$$

The plot of expression presented in Eq. (25) built as a function of time gives a straight line having a gradient of K(T) when the reaction model achieves a successful fit of the data, while the temperature remains constant.

The best model, selected from the best linear regression coefficient of determination (R^2) of the plots, was used to predict the reaction mechanism and to calculate the reaction parameters, e.g., temperature-dependent rate constant and activation energy, by applying Eq. (5). Taking the natural logarithm on both sides and arranging the Eq. (5) the following linear equation shown as Eq. (26) can be obtained.

$$\ln K(T) = -\frac{E_a}{R}\cdot\frac{1}{T} + \ln K_0 \tag{26}$$

A dependence of ln K(T) versus 1/T can be plotted, and a linear regression can be performed after the rate constants have been determined for a reaction carried out at different temperatures and equilibrium pressures. The slope of the line is -Ea/R, and the intercept with Y axis is ln K_0.

3. Results and discussion

3.1. PCT studies and stepwise kinetics measurements

The hydrogen storage capacity of approximately 1.07 (H/M) or 1.6 (wt% H) was achieved when absorbing hydrogen by the studied alloy at room temperature. A small hysteresis was observed between the absorption and desorption profiles, as is seen in the pressure–composition–temperature (PCT) diagram presented in Fig. 1. The details of the kinetics measurements at 273 K, 293 K, 323 K, and 353 K are shown in the Supplementary Information file (Figs. S1–S4). Each experiment is named as related to the measurements parameters. The label 'a' refers to absorption, while 'd' refers to desorption. The name with the label 'c' indicates a complete absorption/desorption measurement; otherwise, a stepwise absorption/desorption was applied. From the graph, we can see that at a higher initial pressure, the reaction occurs faster, as indicated by the broader concentration changes achieved in one second - the measurements time interval.

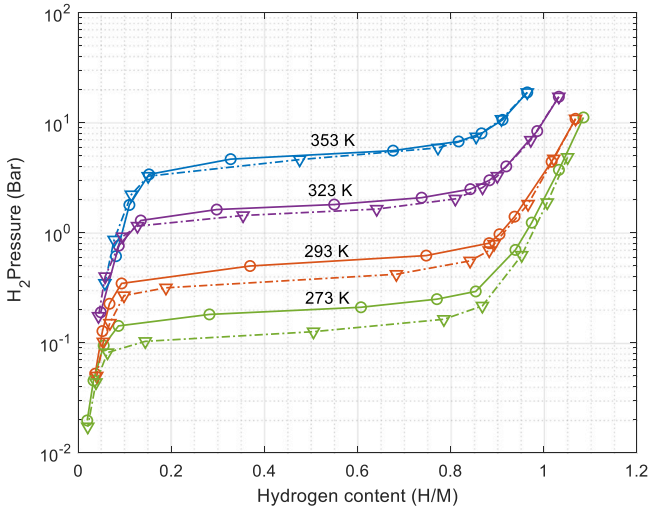

Fig. 1. PCT isotherms for the studied $AB_{1.95}$ alloy were measured at four different temperatures and plotted in a logarithmical scale, absorption data (circle), and desorption data (downward-pointing triangles).

The alloy shows rapid kinetics of H_2 absorption, so the use of stepwise and full absorption characterization with the utilization of a thermal ballast (nickel foam) are both relevant, allowing to prevent a significant temperature increase/decrease during absorption/desorption. The observed increase in temperature was relatively small, less than 1°K, for both stepwise and full H_2 absorption (Fig. 2) experiments thanks to the use of a thermal ballast. Such a technique mitigates the possibility for the excessive inaccuracy of the analysis at the setpoint temperatures by maintaining close to isothermal experimental conditions.

3.2. PCT model

K(P) is a pressure-dependent rate term and is a function of both P (current pressure) and P_{eq} (equilibrium pressure), as it follows from the Eqs. (6)–(20). The difference in pressure between P and P_{eq} is considered as a driving force of the reaction. In the plateau region, it is reasonably accurate to use a linear interpolation between the measured PCT data points to derive the value for the P_{eq} at corresponding hydrogen concentration (in the case when the plateau has a slope). However, this approach will give a significant error when determining the P_{eq} for the full absorption, where the experimental data contains two turning curves before and after the plateau. Because of that reason, in the present work, the equilibrium pressure is defined from the experimental PCT data.

A rational function f(x) has a numerator and denominator of a 3rd-degree expression as presented in Eq. (27). This expression has been selected because the PCT mathematical model gave excellent goodness of fit value at every temperature and in a selected concentration range. It also produces a straight line and slopy plateau as compared to the polynomial, which generates a wavy plateau.

$$f(x) = \frac{(p1\quad x^3+p2\quad x^2+p3\quad x+p4)}{(x^3+q1\quad x^2+q2\quad x+q3)} \tag{27}$$

Here, x is the hydrogen concentration, and it is possible to calculate P_{eq} for any concentration by using that function. The excellent goodness of fit parameter and the graph displayed in Fig. 3 shows that the model describes the PCT data (P_{eq}) well. The rational coefficients are derived by fitting the PCT data with the rational functions until the best goodness of fit is achieved. The coefficients obtained from the fitting are listed in Table S1 of the Supplementary Material. The equilibrium pressure at any point in the range of storage capacity can be derived from this simple equation. We note that

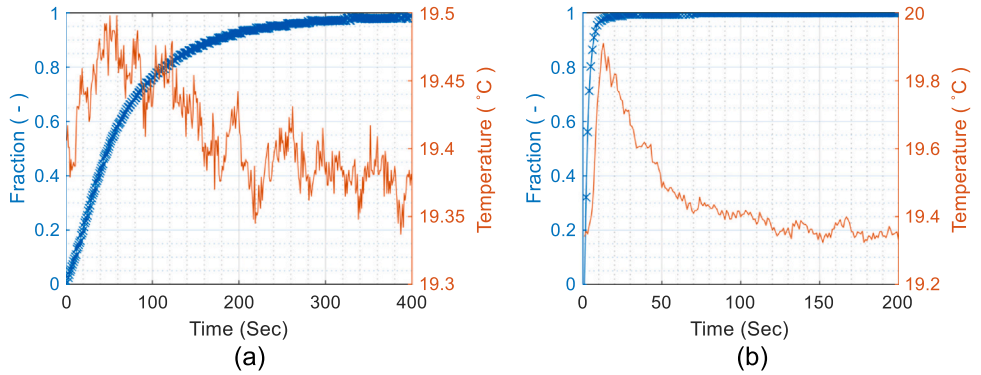

Fig. 2. Temperature profiles during hydrogen absorption in a stepwise (a) and full (b) H_2 absorption experiments. This full absorption temperature profile example is selected for the fastest reaction among the measured data, which allows in just 9 s to achieve a reacted fraction of 0.95. The measured temperature difference was reasonably small, less than 1°K.

the applied PCT model is simple and can be used as an alternative besides the models proposed in the reference data [34–37]. We note that interpolation between the fitted curves generates the P_{eq} data at any concentration and temperature, as shown in Fig. 4.

3.3. Enthalpy and entropy changes during the hydrogenation-dehydrogenation

Equilibrium pressure was selected from the center of the plateau of the PCT model. By plotting the equilibrium pressure vs. 1/T, we obtained van't Hoff plots shown in Fig. 5. The enthalpy change (ΔH) and the entropy change (ΔS) were calculated as $\Delta H_{abs} = -32.20$ kJ/mol H_2, $\Delta H_{des} = 36.03$ kJ/mol H_2, $\Delta S_{abs} = -104.76$ J/K mol H_2, and $\Delta S_{des} = 115.08$ J/K mol H_2. A critical temperature T_c where the two-phase region ends can be found by extrapolating the absorption and desorption pressure dependencies to reach their intercept. It was found that the intercept occurred at the critical temperature of $T_c = 371$ K.

The calculated parameters describing the thermodynamics of H_2 desorption were compared with the results of an earlier work by Wijayanti et al. [18] involving the PCT modeling [27]. The results are compared in Table 2 and show that the current method, using a more convenient and simple procedure, gives the result differing by a maximum of 2% as compared to the reported in [18] values.

The metal hydride studied in this work has negative ΔH and ΔS values, which are typical for the exothermic hydrogen absorption interaction with equilibrium H_2 pressure close to the ambient pressure at room temperature. Naturally, the desorption reaction appears to be endothermic with similar values but opposite in signs ΔH and ΔS.

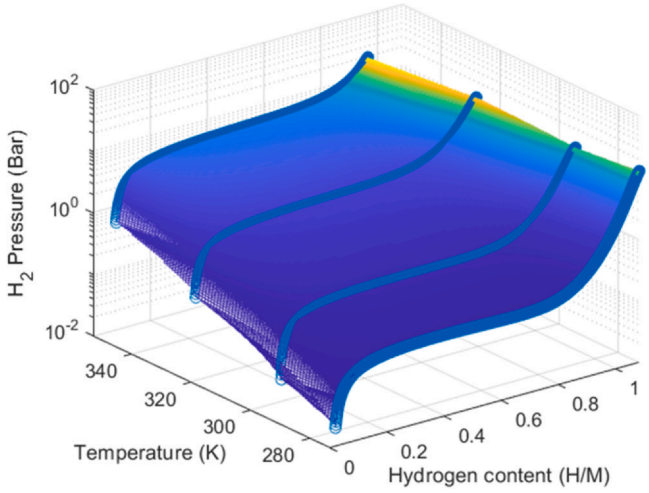

Fig. 4. PCT model of the experimental data for hydrogen absorption that can be generated by grid interpolation from the fitted curve of the experimental data measured at several temperatures.

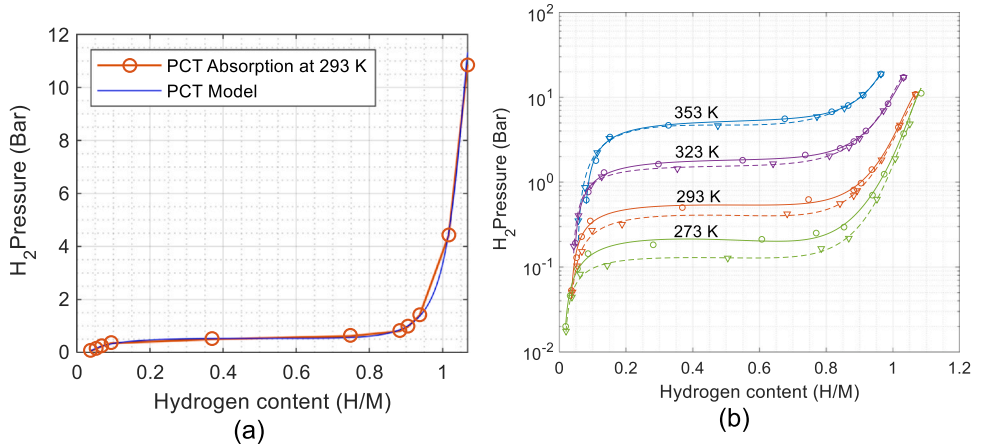

Fig. 3. PCT experimental data and PCT model / theoretical fit of equilibrium pressures using a 3rd-degree rational function of concentration (H/M) for hydrogen absorption at 293 K (a). The modeling data at four selected temperatures, absorption data (circle), absorption model (line), desorption data (downward-pointing triangles), and desorption model (dashed line) plotted in a log scale (b). The PCT model shows excellent goodness of fit for the PCT experimental data.

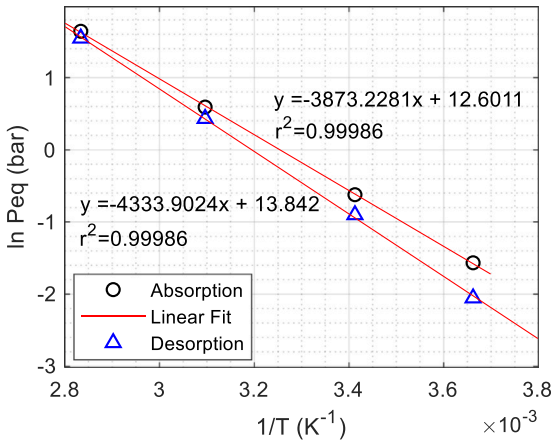

Fig. 5. The van't Hoff plot showing absorption and desorption pressure equilibria vs. inverse temperature. Intersect of the straight lines for absorption and desorption dependencies gives a critical temperature.

Table 2
Comparison of the reference data and the current results for the hydrogen desorption measured for the $Ti_{0.15}Zr_{0.85}La_{0.03}Ni_{1.126}Mn_{0.657}V_{0.113}Fe_{0.113}H_{<3}$ metal hydride.

Properties	Reference data[18]	Current work
-ΔH, kJ/mol H_2	35.25	36.03
-ΔS, J/mol H_2 K	113.33	115.08
T_C, K	370	371

3.4. Effect of temperature and pressure

The effect of temperature on the overall rates of hydrogen absorption and desorption is shown in Fig. 6. It can be seen that during the hydrogen absorption (Fig. 6a) the highest rates are observed at the lowest temperature of 293 K. These rates gradually decrease when the temperature rises first to 323 K and then to 353 K. An opposite dependence was found for the hydrogen desorption (Fig. 6b) with the fastest process taking place at 353 K. The slowest desorption proceeds at 293 K. This temperature-dependent data was measured at approximately the same initial hydrogen pressure. When the higher temperature was applied, the overall absorption reaction rate was relatively low, but the desorption reaction rate was higher. This is related to the thermodynamic driving force for hydrogen absorption as at high temperature, the $P_{eq.}$ is higher while the value of the applied pressure becomes relatively close to P_{eq}, so their difference defining the thermodynamic driving force decreases. Thus the effect of thermodynamic driving force becomes limited in these measurements. In contrast, for the desorption process, the pressures during the experiment are far from the equilibrium pressure. This difference is always quite significant. Consequently, the data presented in Fig. 6 is not entirely quantitatively comparable for the various data sets until this data becomes corrected to account for a pressure-dependent driving force, e.g., by introducing a pressure-dependent rate term.

The pressure dependence of absorption and desorption rates is shown in Fig. 7. This data was collected at a constant temperature of 293 K by varying the initial pressure. We can see that the increase in pressure increases the absorption rate and decreases the desorption rate, as can be seen from the gradient of the curve and the time required to achieve a certain reaction fraction.

The reacted fraction was calculated using Eqs. (2) and (3). Fig. S5 shows the data of the stepwise kinetics measurements at plateaux (a) and (b), and the data of the kinetics measurements during a full absorption (c), and (d). It shows that the reacted fraction as a function of time is affected by both temperature and pressure. Due to the change of the equilibrium pressure, as it changes with the temperature, the temperature-dependent data cannot be obtained at the same pressure. This implies that the reacted fraction curves are difficult to quantitatively compare with each other by a direct comparison.

In order to analyze the effect of temperature and pressure, we have to identify the best fit for the mathematical models of the reaction presented in Table 1 and to explore the temperature and pressure dependence of the reaction rates at the same time.

3.5. Model selection based on simulation results

It is worth applying computerized programming to describe the experimental data collected for the studied hydrogen storage alloy. The description uses various possible rate laws described by the JMAK reaction model (with n = 0.5–4) and other rate laws mentioned in Table 1, in combination with various possible pressure dependences of the rates described in Eqs. (6–20). We will consider as an example an application of the a1 kinetics modeling data at temperature 293 K, see Fig. 8. This data is chosen as an example to characterize K(P) as a driving force of the transformation at the beginning of the plateau during the hydrogen absorption.

When we apply the reaction model presented in Table 1 to the fitting of the data from the experiments, this results in various goodnesses of fit (see detailed results in Supplementary Information, Figs. S7–S21). As shown in Fig. 9, for the studied alloy, the reaction mechanism was most successfully fitted with JMAK model with n = 1, describing the first-order transformation fraction-time curve.

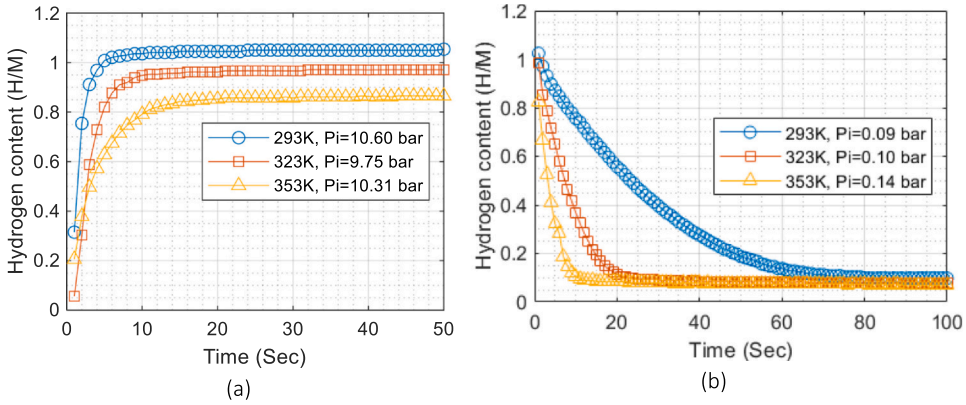

Fig. 6. Hydrogen storage capacity as a function of time for H_2 absorption (a) and desorption (b) at various temperatures starting almost at the same initial pressure (Pi). It shows that the higher temperature makes the absorption slower, and the desorption gets faster; however, we should carefully account for the equilibrium pressure change due to the variations of temperature.

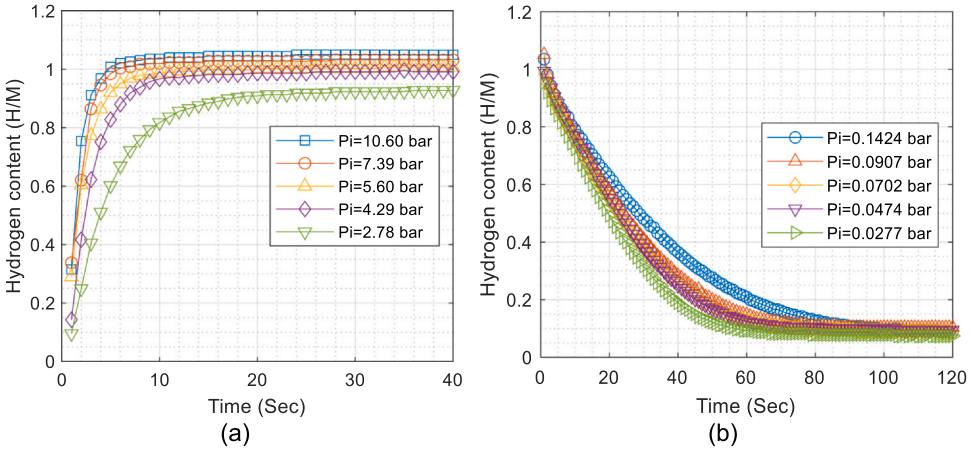

Fig. 7. Hydrogen content as a function of time for absorption (a) and desorption (b) at 293 K at various initial pressures P_i). An increase in pressure increases the absorption rate and decreases the desorption rate.

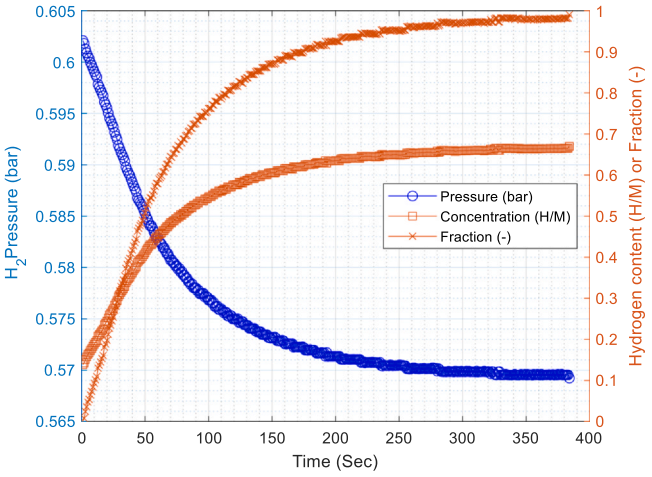

Fig. 8. Kinetics data (pressure, hydrogen content) plotted with calculated reacted fractions using Eq. (2). Kinetics data at 293 with label a1. Data in the range of the reacted fraction from 0 until ± 0.9 is chosen to avoid a decay region.

The modeling of the experimental data can be categorized into three groups: the areas of low H concentration (a reaction that occurs at the beginning of the plateau), medium H concentration (a reaction at the middle of the plateau), and high H concentration (a reaction at the end of the plateau). Data points in the range of the reacted fraction from X = 0 until X = 0.9 are chosen to be within the model limits region. The modeling was done by iterating the parameters of the reaction model g(X) listed in Table 1 (with n = 0.5 to n = 4 for the JMAK model) and pressure-dependent term K(P) from Eqs. (6)–(20).

The JMAK reaction model, in Table 1, with n value 1–1.25 with and K(P) model formulated in the Eq. (14) was selected as the most suitable reaction model. This indicates that the rate-limiting steps of hydrogen absorption and desorption are jointly governed by hydrogen diffusion and grain boundary nucleation of the alpha-solid solution and beta-hydride. During the modeling, the reaction model and the pressure-dependent term were evaluated by comparing the refined values of the coefficient of determination (R-squared value). The best R-squared values for the selected models are listed in Table 3 (absorption) and Table 4 (desorption). R squared values exceeding 0.93 for absorption and 0.90 for desorption were achieved, showing successful fits for the chosen models.

The temperature-dependent rate term increases with the increase of the temperature. Pearson correlation coefficient for the temperature-dependent rate term K(T) for four different temperatures shows R^2 values exceeding 0.92 for absorption and R^2 higher than 0.93 for desorption.

The effect of temperature can be seen from the values of temperature rate term K(T) in Tables 3 and 4, which always increases with the temperature increase. This indicates that the reaction proceeds faster at a higher temperature. However, the increasing temperature increases the pressure, which approaches equilibrium pressure, and therefore the reaction rates tend to decrease. Combining this characteristic with the data of Fig. 6 implies that H_2 absorption is mostly sensitive to pressure changes while desorption is most susceptible to the temperature changes.

3.6. Reaction mechanism and parameters

According to the results obtained from the model simulations, the reaction follows the JMAK model with the value of exponent n 1–1.25 for absorption and 1 for desorption. These refined values of n indicate that the rate-limiting steps of hydrogen absorption and desorption can be jointly governed by hydrogen diffusion and grain boundary nucleation of alpha-solid solution and beta-hydride; see [20] for further details.

This conclusion is furthermore supported by the value of the pressure-dependent term K(P), which is most successfully described using the Eq. (14), indicating that the rate-limiting step is nucleation and growth in the alfa and beta phases [28]. This is observed for both the hydrogenation and dehydrogenation processes. By using the temperature-dependent term K(T) from the model simulation, the corresponding parameters can be obtained using Eq. (26). The activation energy is in the range of 7–33 kJ/mol H_2, as listed in Tables 5 and 6.

The results presented in Tables 5 and 6 show that the activation energies for both hydrogen absorption and desorption decrease during the stepwise hydrogen absorption and desorption. Hydrogen absorption kinetics increases when the alloy contains absorbed hydrogen. For the hydrogenated material that already has some hydrogen, hydrogen uptake proceeds progressively easier. However, it seems to contradict to the experimental results for the hydrogen absorption performed in a single-step process. The kinetics was much easier with a small value of activation energy, only 11 kJ/mol. This is probably caused by use of non-isothermal temperature conditions during the single-step process. The heat generated during the single-step absorption is much higher than that during the stepwise experiments thus causing the temperature swings. The trend observed during the desorption is similar to the one during the hydrogen absorption due to a similar valid model that governs the

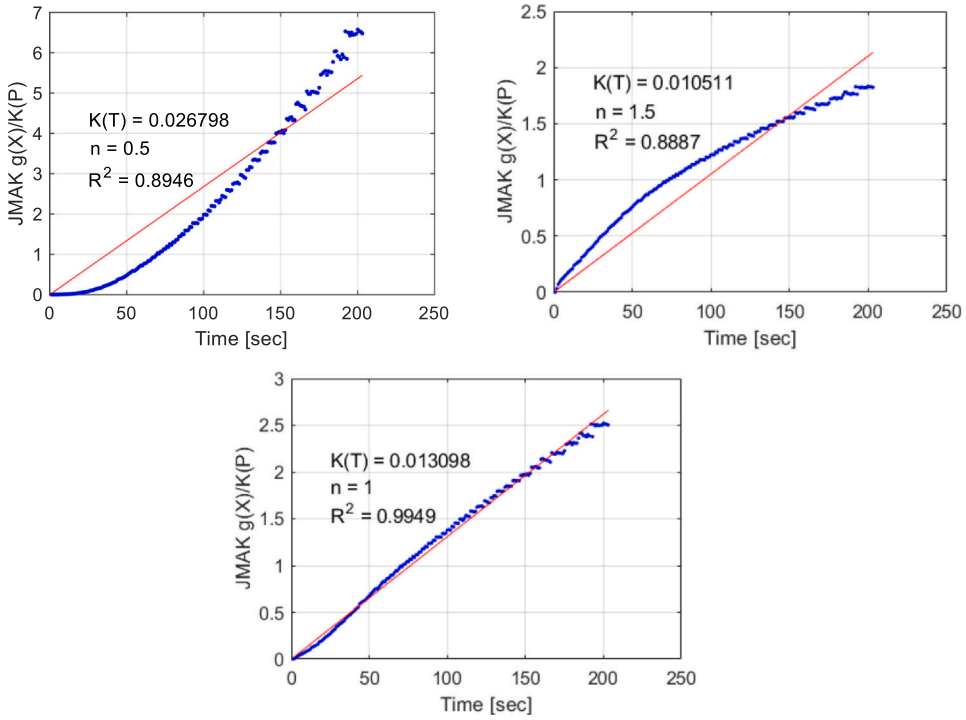

Fig. 9. The fits for the various values of n are compared in this figure. The best fit was achieved when the g(X)=JMAK with n = 1 and $K(P) = \left(\frac{P}{Peq}\right)^{0.5}$. The fitting results are listed in the Supplementary Information file, Figs. S7–S21. The graph gives a value of K(T), which can be found from the value of gradient at the intercept of the fitted line with zero.

reaction mechanism. Nevertheless, further studies are required to explain the observed phenomena.

Up to now, there are no reference studies on the activation energy of hydrogen absorption-desorption for the alloy used in the current study, $Ti_{0.15}Zr_{0.85}La_{0.03}Ni_{1.126}Mn_{0.657}V_{0.113}Fe_{0.113}$. However, Cui et al. [38] reported the valued of activation energies for several Zr-based AB_2 type Laves phase alloys which were 29.3 kJ/mol H_2 for $Ti_{0.1}Zr_{0.9}Mn_{0.9}V_{0.1}Fe_{0.5}Co_{0.5}$, 43.8 kJ/mol H_2 for $Ti_{0.1}Zr_{0.9}(Mn_{0.9}V_{0.1})_{1.1}Fe_{0.5}Ni_{0.5}$, and 48.5 kJ/mol H_2 for $Ti_{0.1}Zr_{0.9}Mn_{0.9}V_{0.1}Fe_{0.55}Ni_{0.55}$. This implies that activation energy determined in this work shows a reasonably good agreement with this reference data.

Table 3
Simulation results for H_2 absorption.

Experiment type	Concentration	Parameters	Temperature			
			273 K	293 K	323 K	353 K
Stepwise absorption	Low H concentration	Experimental data	a1	aa1	a1	a1
		K(P)	$(P/Peq)^{0.5}$	$(P/Peq)^{0.5}$	$(P/Peq)^{0.5}$	$(P/Peq)^{0.5}$
		X	0–0.92	0–0.91	0–0.91	0–0.90
		n	1	1	1	1
		K(T)	0.00593	0.00954	0.05940	0.06160
		R^2	0.99	0.99	1.00	0.96
	Medium H concentration	Experimental data	a2	a1	a2	a2
		K(P)	$(P/Peq)^{0.5}$	$(P/Peq)^{0.5}$	$(P/Peq)^{0.5}$	$(P/Peq)^{0.5}$
		X	0–0.90	0–0.92	0–0.91	0–0.92
		n	1	1	1	1
		K(T)	0.00746	0.01310	0.06030	0.06499
		R^2	0.98	0.99	1.00	0.98
	High H concentration	Experimental data	a3	a2	a4	a3
		K(P)	$(P/Peq)^{0.5}$	$(P/Peq)^{0.5}$	$(P/Peq)^{0.5}$	$(P/Peq)^{0.5}$
		X	0–0.91	0–0.92	0–0.91	0–0.89
		n	1	1	1	1
		K(T)	0.00867	0.03269	0.06845	0.08987
		R^2	0.99	0.99	0.96	0.94
Full hydrogen absorption		Experimental data	ac2	ac8	ac1	ac2
		K(P)	$(P/Peq)^{0.5}$	$(P/Peq)^{0.5}$	$(P/Peq)^{0.5}$	$(P/Peq)^{0.5}$
		X	0–0.95	0–0.95	0–0.94	0–0.95
		n	1.25	1.25	1.25	1.25
		K(T)	0.05868	0.09805	0.13113	0.18146
		R^2	0.93	0.99	0.98	0.98

Table 4
Computer simulation results for H_2 desorption.

Experiment type	Concentration	Parameters	Desorption			
			273 K	293 K	323 K	353 K
Stepwise desorption	Low H concentration	Experimental data	d3	d3	d3	d3
		K(P)	$(P/Peq)^{0.5}$	$(P/Peq)^{0.5}$	$(P/Peq)^{0.5}$	$(P/Peq)^{0.5}$
		X	0–0.95	0–0.90	0–0.91	0–0.91
		n	1	1	1	1
		K(T)	0.00846	0.01014	0.08112	0.15844
		R^2	0.99	0.92	0.97	0.99
	Medium H concentration	Experimental data	d2	d2	d2	d2
		K(P)	$(P/Peq)^{0.5}$	$(P/Peq)^{0.5}$	$(P/Peq)^{0.5}$	$(P/Peq)^{0.5}$
		X	0–0.95	0–0.95	0–0.93	0–0.91
		n	1	1	1	1
		K(T)	0.00699	0.01276	0.06225	0.05955
		R^2	0.99	0.98	0.97	0.96
	High H concentration	Experimental data	d1	d1	d1	d1
		K(P)	$(P/Peq)^{0.5}$	$(P/Peq)^{0.5}$	$(P/Peq)^{0.5}$	$(P/Peq)^{0.5}$
		X	0–0.85	0–0.86	0–0.91	0–0.85
		n	1	1	1	1
		K(T)	0.00876	0.01542	0.06205	0.10096
		R^2	0.90	0.92	0.96	0.92
Full hydrogen desorption		Experimental data	dc2	dc10	dc6	dc4
		K(P)	$(P/Peq)^{0.5}$	$(P/Peq)^{0.5}$	$(P/Peq)^{0.5}$	$(P/Peq)^{0.5}$
		X	0–0.95	0–0.95	0–0.95	0–0.95
		n	1	1	1	1
		K(T)	0.01975	0.04460	0.16695	0.49233
		R^2	0.99	1.00	0.97	0.96

Table 5
Kinetic parameters for hydrogen absorption.

Parameter	Stepwise absorption			Full hydrogen absorption	Units
	Low H concentration	Medium H concentration	High H concentration		
n	1	1	1	1.25	–
Ea	27	24	23	11	kJ mol^{-1}
Ko	685	294	274	7	s^{-1}
K(P)	$(P/Peq)^{0.5}$	$(P/Peq)^{0.5}$	$(P/Peq)^{0.5}$	$(P/Peq)^{0.5}$	–

Table 6
Kinetic parameters for hydrogen desorption.

Parameter	Stepwise desorption			Full hydrogen desorption	Units
	Low H concentration	Medium H concentration	High H concentration		
n	1	1	1	1	–
Ea	33	26	26	33	kJ mol^{-1}
Ko	11,079	692	793	30,884	s^{-1}
K(P)	$(P/Peq)^{0.5}$	$(P/Peq)^{0.5}$	$(P/Peq)^{0.5}$	$(P/Peq)^{0.5}$	–

4. Conclusions

The hydrogen absorption and desorption kinetics in $Ti_{0.15}Zr_{0.85}La_{0.03}Ni_{1.126}Mn_{0.657}V_{0.113}Fe_{0.113}$ – H_2 system were investigated. The experiments were conducted using a single-step absorption and desorption and stepwise methods. Both hydrogen absorption and desorption proceed faster with increasing temperature as indicated by the increase of the temperature rate term K(T), except when the thermodynamics influences the rates of the absorption process at pressures close to the equilibrium conditions. The absorption and desorption proceed faster when increasing the operating H_2 pressure and H_2 pressure difference with equilibrium pressure of the hydride formation. The effect is more evident at low temperatures for absorption and high temperatures for desorption.

We found that the values of exponent n in the kinetic equation defining the rate of hydrogenation-dehydrogenation was in a range 1–1.25. These indicates that the rate-limiting hydrogen absorption and desorption steps can be jointly governed by hydrogen diffusion and grain boundary nucleation of alpha-solid solution and beta-hydride. The pressure-dependent kinetic model was selected as the most suitable model and well described the experimental data during the simulations, which defines that nucleation and growth of the alfa and beta phases as the rate-limiting step.

The activation energies well agree with the values reported in the literature for the hydrides of the related Zr-based AB_2 type Laves phase alloys. The $\Delta H_{abs.}$ 36.03 kJ/mol H_2 and $\Delta S_{abs.}$ 115.08 J/mol H_2 K obtained during the studies of the thermodynamics of hydrogen desorption show an excellent agreement with the earlier reported values obtained in the independent studies by using different techniques (within a margin of just 2%). The activation energies for both absorption and desorption decrease along with increasing hydrogen concentration in the hydride during the stepwise experiments.

Obtained data of the experimental studies and theoretical modeling of the kinetics, thermodynamics, and studies of the mechanism of the phase structural transformations during the hydrogenation-dehydrogenation are expected to have a significant value when modeling and optimizing the performance of low-pressure hydrogen

tanks accommodating the developed alloy in order to achieve the most efficient temperature-dependent rates of hydrogen charge and discharge in the H storage systems.

CRediT authorship contribution statement

Arif Hariyadi, Suwarno Suwarno, Roman V. Denys, Jose Bellosta von Colbe: Conceptu alization, Methodology, Software, Writing – review & editing. **Arif Hariyadi, Suwarno Suwarno, Volodymyr Yartys:** Data curation, Writing – original draft preparation. **Arif Hariyadi, Roman V. Denys:** Visualization, Investigation. **Tor Oskar Sætre, Volodymyr Yartys, Jose Bellosta von Colbe:** Supervision. **Arif Hariyadi, Roman V. Denys, Jose Bellosta von Colbe, Suwarno Suwarno:** Software, Validation. **Arif Hariyadi, Suwarno Suwarno, Tor Oskar Sætre, Volodymyr Yartys:** Writing – review & editing.

Declaration of Competing Interest

The authors declare that they have no known competing financial interests or personal relationships that could have appeared to influence the work reported in this paper.

Acknowledgments

This work received a support from the EU Horizon 2020 program by the European Comission in the H2020-MSCARISE-2017 action, HYDRIDE4MOBILITY project, with Grant Agreement 778307. Suwarno Suwarno and Arif Hariyadi thank the Ministry of Research, Culture, and Education of Indonesia, for the funding received from Fundamental Research Grant Number 783/PKS/ITS/2021.

Appendix A. Supporting information

Supplementary data associated with this article can be found in the online version at doi:10.1016/j.jallcom.2021.162135.

References

[1] D. Gielen, F. Boshell, D. Saygin, M.D. Bazilian, N. Wagner, R. Gorini, The role of renewable energy in the global energy transformation, Energy Strategy Rev. 24 (2019) 38–50, https://doi.org/10.1016/j.esr.2019.01.006

[2] J.P. Vanhanen, P.D. Lund, J.S. Tolonen, Electrolyser-metal hydride-fuel cell system for seasonal energy storage, Int. J. Hydrog. Energy 23 (1998) 267–271, https://doi.org/10.1016/S0360-3199(97)00065-7

[3] J. Bellosta von Colbe, J.-R. Ares, J. Barale, M. Baricco, C. Buckley, G. Capurso, N. Gallandat, D.M. Grant, M.N. Guzik, I. Jacob, E.H. Jensen, T. Jensen, J. Jepsen, T. Klassen, M.V. Lototskyy, K. Manickam, A. Montone, J. Puszkiel, S. Sartori, D.A. Sheppard, A. Stuart, G. Walker, C.J. Webb, H. Yang, V. Yartys, A. Züttel, M. Dornheim, Application of hydrides in hydrogen storage and compression: achievements, outlook and perspectives, Int. J. Hydrog. Energy 44 (2019) 7780–7808, https://doi.org/10.1016/j.ijhydene.2019.01.104

[4] L.J. Bannenberg, M. Heere, H. Benzidi, J. Montero, E.M. Dematteis, S. Suwarno, T. Jaroń, M. Winny, P.A. Orłowski, W. Wegner, A. Starobrat, K.J. Fijałkowski, W. Grochala, Z. Qian, J.-P. Bonnet, I. Nuta, W. Lohstroh, C. Zlotea, O. Mounkachi, F. Cuevas, C. Chatillon, M. Latroche, M. Fichtner, M. Baricco, B.C. Hauback, A.E. Kharbachi, Metal (boro-) hydrides for high energy density storage and relevant emerging technologies, Int. J. Hydrog. Energy 45 (2020) 33687–33730, https://doi.org/10.1016/j.ijhydene.2020.08.119

[5] M.V. Lototskyy, I. Tolj, L. Pickering, C. Sita, F. Barbir, V. Yartys, The use of metal hydrides in fuel cell applications, Prog. Nat. Sci.: Mater. Int. 27 (2017) 3–20, https://doi.org/10.1016/j.pnsc.2017.01.008

[6] M.V. Lototskyy, M.W. Davids, I. Tolj, Y.V. Klochko, B.S. Sekhar, S. Chidziva, F. Smith, D. Swanepoel, B.G. Pollet, Metal hydride systems for hydrogen storage and supply for stationary and automotive low temperature PEM fuel cell power modules, Int. J. Hydrog. Energy 40 (2015) 11491–11497, https://doi.org/10.1016/j.ijhydene.2015.01.095

[7] Y. Pang, Q. Li, A review on kinetic models and corresponding analysis methods for hydrogen storage materials, Int. J. Hydrog. Energy 41 (2016) 18072–18087, https://doi.org/10.1016/j.ijhydene.2016.08.018

[8] B.P. Tarasov, A.A. Arbuzov, S.A. Mozhzhuhin, A.A. Volodin, P.V. Fursikov, M.V. Lototskyy, V.A. Yartys, Hydrogen storage behavior of magnesium catalyzed by nickel-graphene nanocomposites, Int. J. Hydrog. Energy 44 (2019) 29212–29223, https://doi.org/10.1016/j.ijhydene.2019.02.033

[9] B. Liu, B. Zhang, Y. Wu, W. Lv, S. Zhou, Theoretical prediction and experimental study on catalytic mechanism of incorporated Ni for hydrogen absorption of Mg, Int. J. Hydrog. Energy 44 (2019) 27885–27895, https://doi.org/10.1016/j.ijhydene.2019.09.045

[10] B. Zhang, Y. Lv, J. Yuan, Y. Wu, Effects of microstructure on the hydrogen storage properties of the melt-spun Mg-5Ni-3La (at%) alloys, J. Alloy. Compd. 702 (2017) 126–131, https://doi.org/10.1016/j.jallcom.2017.01.221

[11] S. Suwarno, J.K. Solberg, J.P. Maehlen, B. Krogh, V.A. Yartys, The effects of rapid solidification on microstructure and hydrogen sorption properties of binary BCC Ti–V alloys, J. Alloy. Compd. 582 (2014) 540–546, https://doi.org/10.1016/j.jallcom.2013.08.077

[12] D.G. Ivey, D.O. Northwood, Storing hydrogen in AB $_2$ laves-type compounds*, Z. Für Phys. Chem. 147 (1986) 191–209, https://doi.org/10.1524/zpch.1986.147.1_2.191

[13] J.C. Sun, S. Li, S.J. Ji, The effects of the substitution of Ti and La for Zr in $ZrMn_{0.7}V_{0.2}Co_{0.1}Ni_{1.2}$ hydrogen storage alloys on the phase structure and electrochemical properties, J. Alloy. Compd. 446–447 (2007) 630–634, https://doi.org/10.1016/j.jallcom.2007.03.108

[14] W.-X. Chen, Effects of addition of rare-earth element on electrochemical characteristics of $ZrNi_{1.1}Mn_{0.5}V_{0.3}Cr_{0.1}$ hydrogen storage alloy electrodes, J. Alloy. Compd. 319 (2001) 119–123, https://doi.org/10.1016/S0925-8388(00)01496-1

[15] A.A. Volodin, R.V. Denys, C. Wan, I.D. Wijayanti, Suwarno, B.P. Tarasov, V.A. Yartys, Study of hydrogen storage and electrochemical properties of AB_2-type $Ti_{0.15}Zr_{0.85}La_{0.03}Ni_{1.2}Mn_{0.7}V_{0.12}Fe_{0.12}$ alloy, J. Alloy. Compd. 793 (2019) 564–575, https://doi.org/10.1016/j.jallcom.2019.03.134

[16] C. Wan, R.V. Denys, M. Lelis, D. Milčius, V.A. Yartys, Electrochemical studies and phase-structural characterization of a high-capacity La-doped AB_2 Laves type alloy and its hydride, J. Power Sources 418 (2019) 193–201, https://doi.org/10.1016/j.jpowsour.2019.02.044

[17] K. Young, D.F. Wong, T. Ouchi, B. Huang, B. Reichman, Effects of La-addition to the structure, hydrogen storage, and electrochemical properties of C14 metal hydride alloys, Electrochim. Acta 174 (2015) 815–825, https://doi.org/10.1016/j.electacta.2015.06.048

[18] I.D. Wijayanti, R. Denys, Suwarno, A.A. Volodin, M.V. Lototskyy, M.N. Guzik, J. Nei, K. Young, H.J. Roven, V. Yartys, Hydrides of Laves type Ti–Zr alloys with enhanced H storage capacity as advanced metal hydride battery anodes, J. Alloy. Compd. 828 (2020) 154354, https://doi.org/10.1016/j.jallcom.2020.154354

[19] M. Sato, Studies of hydrogen absorption and desorption processes in advanced intermetallic hydrides, 2005.

[20] T. Førde, J.P. Maehlen, V.A. Yartys, M.V. Lototsky, H. Uchida, Influence of intrinsic hydrogenation/dehydrogenation kinetics on the dynamic behaviour of metal hydrides: a semi-empirical model and its verification, Int. J. Hydrog. Energy 32 (2007) 1041–1049, https://doi.org/10.1016/j.ijhydene.2006.07.015

[21] P.S. Rudman, Hydrogen-diffusion-rate-limited hydriding and dehydriding kinetics, J. Appl. Phys. 50 (1979) 7195–7199, https://doi.org/10.1063/1.325831

[22] M. Martin, C. Gommel, C. Borkhart, E. Fromm, Absorption and desorption kinetics of hydrogen storage alloys, J. Alloy. Compd. 238 (1996) 193–201, https://doi.org/10.1016/0925-8388(96)02217-7

[23] Y. Josephy, M. Ron, Kinetic measurements of $LaNi_5H_x$ and $MmNi_{4.15}Fe_{0.85}H_x$ with constant pressure differentials, J. Less Common Met. 147 (1989) 227–238, https://doi.org/10.1016/0022-5088(89)90196-3

[24] J. Bloch, The kinetics of a moving metal hydride layer, J. Alloy. Compd. 312 (2000) 135–153, https://doi.org/10.1016/S0925-8388(00)01102-6

[25] K. Soo-Ryoung, L. Jai-Young, The effect of thermal cycling on the hydriding rate of MmNi4. 5Al0. 5, J. Less Common Met. 161 (1990) 37–47, https://doi.org/10.1016/0022-5088(90)90312-8

[26] V.M. Skripnyuk, M. Ron, Hydrogen desorption kinetics in intermetallic compounds C2, C51 and C52 with Laves phase structure, Int. J. Hydrog. Energy 28 (2003) 303–309, https://doi.org/10.1016/S0360-3199(02)00081-2

[27] M. Ron, The normalized pressure dependence method for the evaluation of kinetic rates of metal hydride formation/decomposition, J. Alloy. Compd. 283 (1999) 178–191, https://doi.org/10.1016/S0925-8388(98)00859-7

[28] X.-L. Wang, S. Suda, A dehydriding kinetic study of $LaNi_{4.7}Al_{0.3}$ hydride by a stepwise method, J. Less Common Met. 159 (1990) 83–90, https://doi.org/10.1016/0022-5088(90)90135-7

[29] O. Bernauer, J. Töpler, D. Noréus, R. Hempelmann, D. Richter, Fundamentals and properties of some Ti/Mn based Laves phase hydrides, Int. J. Hydrog. Energy 14 (1989) 187–200, https://doi.org/10.1016/0360-3199(89)90053-0

[30] T. Liavitskaya, S. Vyazovkin, Delving into the kinetics of reversible thermal decomposition of solids measured on heating and cooling, J. Phys. Chem. C 121 (2017) 15392–15401, https://doi.org/10.1021/acs.jpcc.7b05066

[31] N. Koga, L. Favergeon, S. Kodani, Impact of atmospheric water vapor on the thermal decomposition of calcium hydroxide: a universal kinetic approach to a physico-geometrical consecutive reaction in solid–gas systems under different partial pressures of product gas, Phys. Chem. Chem. Phys. 21 (2019) 11615–11632, https://doi.org/10.1039/C9CP01327J

[32] S. Vyazovkin, A.K. Burnham, J.M. Criado, L.A. Pérez-Maqueda, C. Popescu, N. Sbirrazzuoli, ICTAC Kinetics Committee recommendations for performing kinetic computations on thermal analysis data, Thermochim. Acta 520 (2011) 1–19, https://doi.org/10.1016/j.tca.2011.03.034

[33] A. Khawam, D.R. Flanagan, Solid-state kinetic models: basics and mathematical fundamentals, J. Phys. Chem. B 110 (2006) 17315–17328, https://doi.org/10.1021/jp062746a

[34] T. Nishizaki, K. Miyamoto, K. Yoshida, Coefficients of performance of hydride heat pumps, J. Less Common Met. 89 (1983) 559–566, https://doi.org/10.1016/0022-5088(83)90372-7

[35] A. Jemni, S.B. Nasrallah, Study of two-dimensional heat and mass transfer during absorption in a metal-hydrogen reactor, Int. J. Hydrog. Energy 20 (1995) 43–52, https://doi.org/10.1016/0360-3199(93)E0007-8
[36] A.T. Wijayanta, K. Nakaso, T. Aoki, Y. Kitazato, J. Fukai, Effect of pressure, composition and temperature characteristics on thermal response and overall reaction rates in a metal hydride tank, Int. J. Hydrog. Energy 36 (2011) 3529–3536, https://doi.org/10.1016/j.ijhydene.2010.12.047
[37] M.V. Lototskyy, New model of phase equilibria in metal–hydrogen systems: features and software, Int. J. Hydrog. Energy 41 (2016) 2739–2761, https://doi.org/10.1016/j.ijhydene.2015.12.055
[38] X.-Y. Cui, Q. Li, K.-C. Chou, S.-L. Chen, G.-W. Lin, K.-D. Xu, A comparative study on the hydriding kinetics of Zr-based AB_2 hydrogen storage alloys, Intermetallics 16 (2008) 662–667, https://doi.org/10.1016/j.intermet.2008.02.009